



Properties of BaTiO₃ confined in nanoporous Vycor and artificial opal silica

Dmitry Nuzhnyy¹, Přemysl Vaněk¹, Jan Petzelt¹, Viktor Bovtun¹, Martin Kempa¹, Ivan Gregora¹, Maxim Savinov¹, Radmila Krupková¹, Václav Studnička¹, Josef Buršík², Mihail I. Samoylovich³, Wilfried Schranz⁴

¹Institute of Physics ASCR, Na Slovance 2, 18221 Praha 8, Czech Republic

²Institute of Inorganic Chemistry ASCR, 250 68 Husinec-Řež, Czech Republic

³Central Research Technological Institute "TECHNOMASH" 4, I. Franco St., 121108 Moscow, Russia

⁴Faculty of Physics, University of Vienna, Boltzmannngasse 5, A-1090 Vienna, Austria

Received 5 March 2010; received in revised form 17 May 2010; accepted 25 July 2010

Abstract

Using the sol-gel technique, BaTiO₃ was embedded into nanoporous Vycor and artificial vitreous opal silica for the first time. About 50 vol% of the pores was filled. In case of the Vycor glass (pore diameter 4–6 nm) only amorphous phase was revealed by XRD, IR reflectivity and Raman spectra. After additional gradual annealing, no crystallization was achieved. Chemical reaction with the SiO₂ skeleton started at ~1000 K. The room-temperature IR and Raman spectra clearly show characteristic vibrational modes of the ferroelectrically distorted TiO₆ octahedra without any long-range order. In case of the opal matrix (densely packed silica spheres, pore diameter up to ~50 nm), crystallization of the ferroelectric BaTiO₃ appeared in coexistence with the amorphous phase, but the penetration depth of the crystalline BaTiO₃ was limited. From the apparent temperature independence of the effective wide-frequency dielectric response due to the essentially temperature independent effective soft mode stiffened to ~100 cm⁻¹, we can deduce that no macroscopic percolation of the crystalline BaTiO₃ has appeared in our opal matrix. Nevertheless, Raman spectra bring evidence of a diffuse ferroelectric phase transition in the opal-BaTiO₃ composite.

Keywords: nanocomposite, confined BaTiO₃, porous silica, stiffened soft mode, effective dielectric properties

1. Introduction

Vycor is a trademark name for a nanoporous vitreous silica (silica glass) known for about 70 years [1]. Its system of pores comprises a complex network of channels with a narrow size distribution within nanometric length limits [2,3]. Considerable effort was devoted to study the dielectric relaxations of liquids confined in these nanopores [4–7] and size effects on the glass transition in organic glass-forming liquids like salol, using dynamic mechanical analysis [8–10].

On the other hand, artificial compact three-dimensional opals have been fabricated relatively recently and only a few composites have been prepared hitherto by

impregnation of the pores, e.g. with magnetic ferrites [11,12]. They consist of a regular monodisperse system of closely packed vitreous spherical silica particles with diameter between 200 and 400 nm.

It is well known that ferroelectrics also change their properties with decreasing particle size and the size effect of ferroelectrics is currently a hot topic quite intensely studied [13]. However, only NaNO₂ ferroelectric, which can be easily infiltrated into the nanopores by melting, was prepared and thoroughly studied as a composite with Vycor-type glasses [14], but no intrinsic confinement effect on the phonons was revealed [15]. In this paper we report for the first time on processing and spectroscopic and dielectric characterization of composites of nanoporous silica matrices with the classic ferroelectric BaTiO₃ (BT) with the aim to study the confinement effect on the ferroelectric phase transition and phonons.

* Corresponding author: tel: +420 266 05 2659
fax: +420 286 89 0415, e-mail: nuzhnyj@fzu.cz

II. Sample preparation

Nanoporous Vycor glass (7930, Corning Inc.) is composed of nearly pure (96–98 %) amorphous silica of 1.5 g/cm³ density with ~28 vol% of pores. The pores form interconnected channels of 4–6 nm diameter and ~30 nm average length. The artificial opal was prepared by sedimentation of amorphous silica nanoballs of ~250 nm diameter with 35–40 vol% porosity with pores of complex topology and sizes from zero up to ~50 nm [11].

Both matrices were filled with BT using the sol-gel technique. The BT sol was prepared from Ti-ethoxide (Ti(OCH₂CH₃)₄, Sigma-Aldrich), Ba-methoxyethoxide (Ba(OCH₂CH₂OCH₃)₂, home-synthesised), acetylacetonate as modifier (molar ratio $n(acac)/n(Ti) = 2$) and methoxyethanol as solvent. Concentration of Ti and Ba in the sol was 0.23 M. The matrix was dried and activated by annealing at 600°C. Then it was repeatedly soaked overnight by BT sol in a Schlenk vessel under dried nitrogen, whipped by paper tissue and annealed in air at 600°C (1 h heating, 1 h dwell, slow free cooling of the furnace to 250°C, rapid cooling after removal from the furnace). Higher annealing temperature during fill-

ing cannot be used because the pore structure of the matrix could be damaged.

On filling-up the 0.44 mm thick Vycor glass sample with BT, the pyrolysis of organics slowed down substantially after the 21st cycle and the soaking - annealing procedure was therefore stopped. The achieved BT concentration in the sample was 32 wt.% so that 42 % of the pore volume was filled up determined by weighing with the BT density $\rho_{BT} = 6.02$ g/cm³ and $\rho_{SiO_2} = 2.2$ g/cm³ (see Fig. 1). It is evident that the filling process slows down with increasing number of soaking cycles. XRD shows amorphous structure of the samples annealed at 600°C (Fig. 2). Indication of the most intense BT diffraction line was present in the as-prepared sample, presumably due to the thin surface film of a partially crystallized BT, but the polished sample shows only amorphous behaviour. Results of the electron probe microanalysis were in good agreement with the desired composition Ba : Ti = 1 : 1 and SiO₂ concentration of 68 wt.%, determined independently by weighing.

Next we tried to crystallize the BT by annealing the as-prepared Vycor-BT sample at 800°C for 1 hour. However, according to XRD, predominantly fresnoite Ba₂TiSi₂O₈ was formed by a chemical reaction of BT with SiO₂. Following stepwise annealing combined with XRD revealed that the sample remained amorphous after annealing up to 700°C and started to react with SiO₂ at 750°C.

In case of the filled-up opal sample (10×10 mm, 2.8 mm thickness), slowing down of the pyrolysis was not observed, but after the 55th soaking cycle it became obvious that a surface layer of BT started to form, despite careful whipping of the sample after soaking. Therefore the soaking-annealing procedure was stopped after the 60th cycle. The sample mass dependence on the number of soaking cycles is also shown in Fig. 1. BT concentration in the sample was 45 wt.% so that 51 % of the pore volume was filled (considering 63 vol% of SiO₂). XRD was carried out with the as-prepared sample and a sample with the surface layer ground off (Fig. 2). It follows from the diffractograms that there was also a layer of crystalline BT on the sample surface (cubic-like, no tetragonal splitting was seen). After grinding off the surface layer (~0.1 mm), both amorphous and crystalline BT phases could be seen. After removal of 0.8 mm thick layer from the other side only amorphous phase was detected (Fig. 2). Therefore it became clear that the crystalline BT concentration in the matrices showed a pronounced depth gradient.

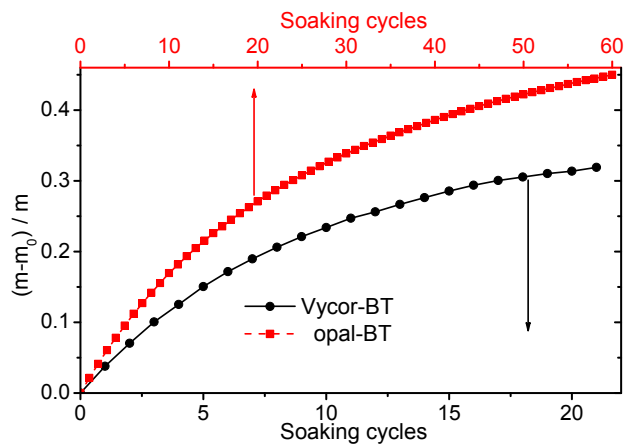


Figure 1. Filling process of BT into nanoporous Vycor and opal matrices - the relative mass filling factor of BT is plotted against the number of soaking cycles

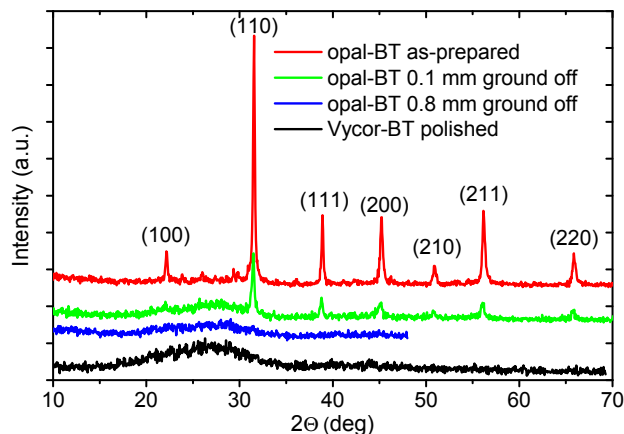


Figure 2. XRD of polished Vycor-BT, as-prepared opal-BT and ground off opal-BT samples

III. Experimental

After preliminary characterization described above, the samples were polished and further studied by infrared (IR) reflectivity (FTIR spectrometer Bruker IFS 113v, specular reflection attachment), time-domain THz transmission spectroscopy (laboratory-made spectrom-

eter based on an amplified Ti-sapphire femtosecond laser system [16]), high-frequency and microwave (MW) dielectric measurements (dielectric spectrometer with Novocontrol BDS 2100 coaxial sample cell and Agilent 4291B impedance analyzer in the 1 MHz–1.8 GHz range and open-end coaxial technique with Agilent E8364B vector network analyzer in the 200 MHz–4 GHz range), standard low-frequency dielectric measurements (dielectric analyzer Novocontrol Alpha AN in the 10^2 – 10^6 Hz range) and Raman scattering (Renishaw RM 1000 Raman microscope, 514.5 nm excitation at 5 mW, Linkam THS600 temperature cell).

IV. Results and discussion

Room-temperature IR reflectivity spectra of our samples are shown in Fig. 3. It is seen that both empty matrices have similar spectra dominated by a single strong band in the 400–500 cm^{-1} range. All other features stem from BT. For the THz transmission measurements it was necessary to prepare a thinner opal-BT sample by grinding off ~ 0.8 mm from one sample side, resulting in a plate of 1.9 mm thickness. The thinner Vycor-BT sample of 0.44 mm thickness was measured in the THz range as prepared. The two IR reflectivity spectra of the opal-BT sample were obtained from both sides of the sample with one side as prepared. They differ strongly from each other, which is obviously due to a different content of BT caused by a pronounced depth gradient of the BT-concentration in our opal-BT sample (at least of its crystalline part). This is clear considering the small effective penetration depths (about tens of μm or less) which take part in the reflectivity values around the absorption peaks. As already mentioned, XRD from this sample side (Fig. 2) has shown that only amorphous BT phase remained in the sample. Some BT-concentration gradient can be obviously expected also in the Vycor-BT sample. This explains why the THz transmission spectra, which probe the BT-concentration averaged over the whole sample volume, yield smaller calculated reflectivity values (Fig. 3) in comparison with the IR reflectivity obtained from the unpolished side, while they are in agreement with the IR reflectivity from the ground off side of the sample.

The reflectivity spectra were fitted with a standard model of the factorized form of generalized oscillators [17] and the fitted reflectivity curves are also shown in Fig. 3. The fit quality is quite good. The calculated complex dielectric functions from the fits are shown in Fig. 4. The mode assignment suggested in Fig. 4 (see the discussion later) is based on IR reflectivity studies on BT ceramics [18] and previous IR studies on BT single crystals [19,20]. It is well known that in the ferroelectric phase the soft TO_1 mode from the paraelectric cubic phase is strongly split into the E and A_1 component, whereas the weak and sharp TO_2 mode is split only negligibly. For the discussion of the effective di-

electric functions in our nanocomposites we tried also to simulate the effective dielectric spectra using the known dielectric functions of both pure components. Two frequently used models of the effective medium have been applied to the Vycor-BT nanocomposite -

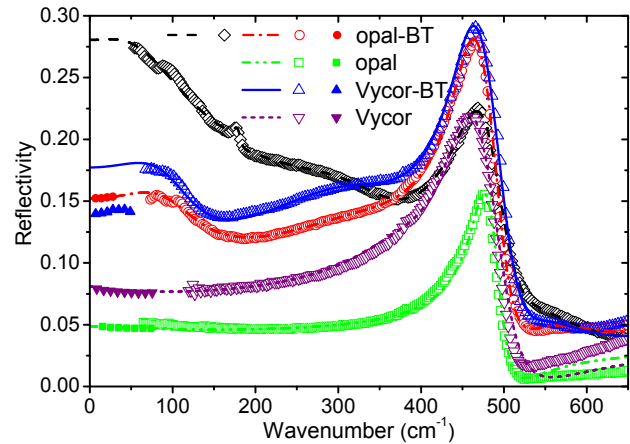


Figure 3. Room temperature IR reflectivity (empty symbols) of Vycor-BT and opal-BT composites compared with the reflectivities of empty Vycor and opal silica matrices. Reflectivity of opal-BT was measured from both sample surfaces (as-prepared \diamond and ground off \circ). Also the reflectivities calculated from the measured THz data (full symbols) and reflectivities from the fits (lines) are presented.

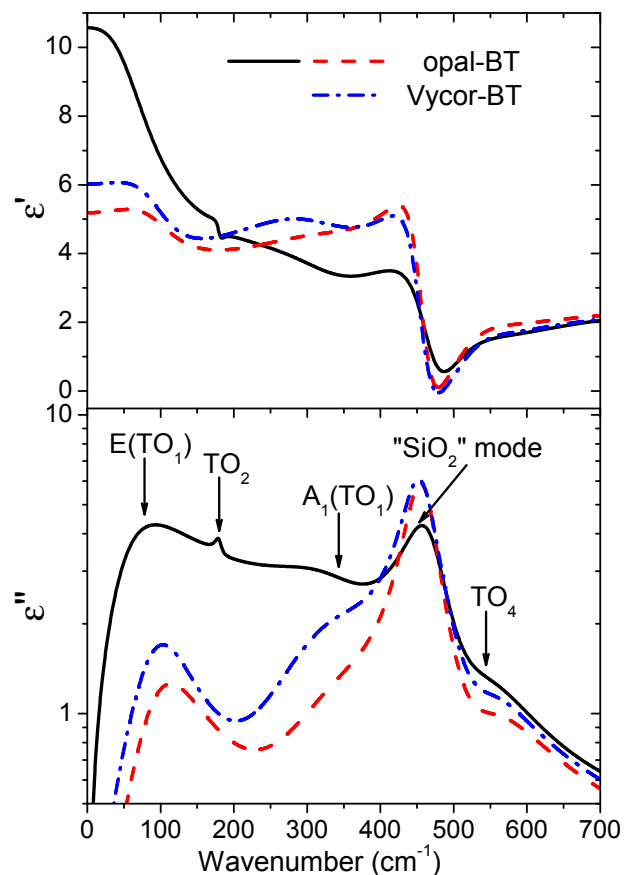


Figure 4. IR complex dielectric functions of the composite samples calculated from the reflectivity fits. For the assignment of phonon modes see [18–20].

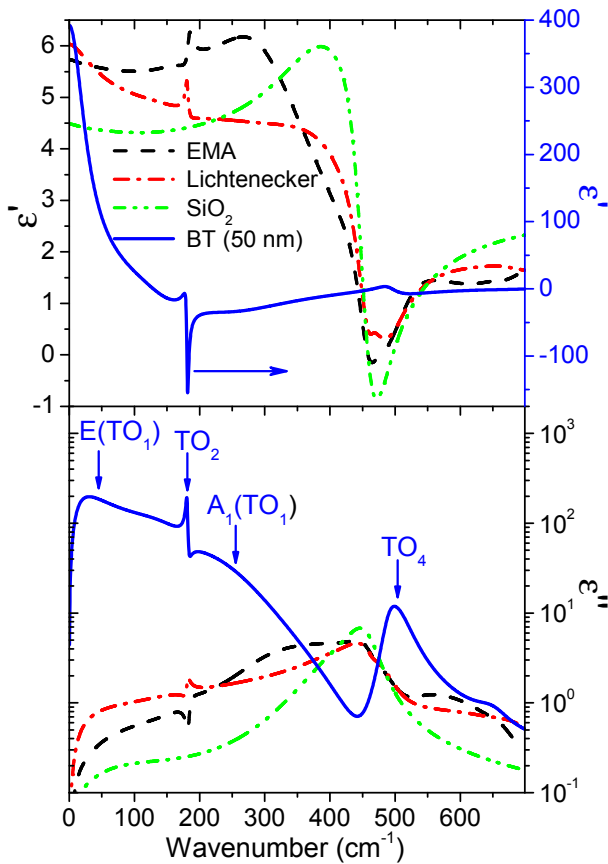


Figure 5. IR dielectric functions of the pure composite components - BT nanoceramics (50 nm grain size) [18] and silica glass, calculated from the empty Vycor reflectivity considering its porosity using Bruggeman EMA model, and the effective dielectric functions of the Vycor-BT composite calculated by two models - Bruggeman and Lichtenecker

Bruggeman effective medium approximation (EMA) and Lichtenecker model [21]. First, the dielectric response of fully dense silica glass was obtained from fitting the IR reflectivity of empty Vycor glass by using the Bruggeman model considering 28 % air porosity. Then we have used the room-temperature dielectric function of dense BT nanoceramics with ~50 nm grain size [22,23] and the effective response of our composite was calculated using the Bruggeman and Lichtenecker mixing formula taking 16 vol% of the BT concentration. The dielectric functions of both pure components and the two above-mentioned effective dielectric functions are presented in Fig. 5. Comparison with the dielectric functions of our composites in Fig. 4 from the reflectivity fits shows a qualitative agreement, which will be discussed below.

In Fig. 6 we summarize our high-frequency room-temperature dielectric measurements in a broad frequency range of 10^6 – 10^{12} Hz, obtained by three different techniques without electrodes. In the open-end coaxial technique, the E -field is approximately parallel to the sample surface and has a small penetration depth

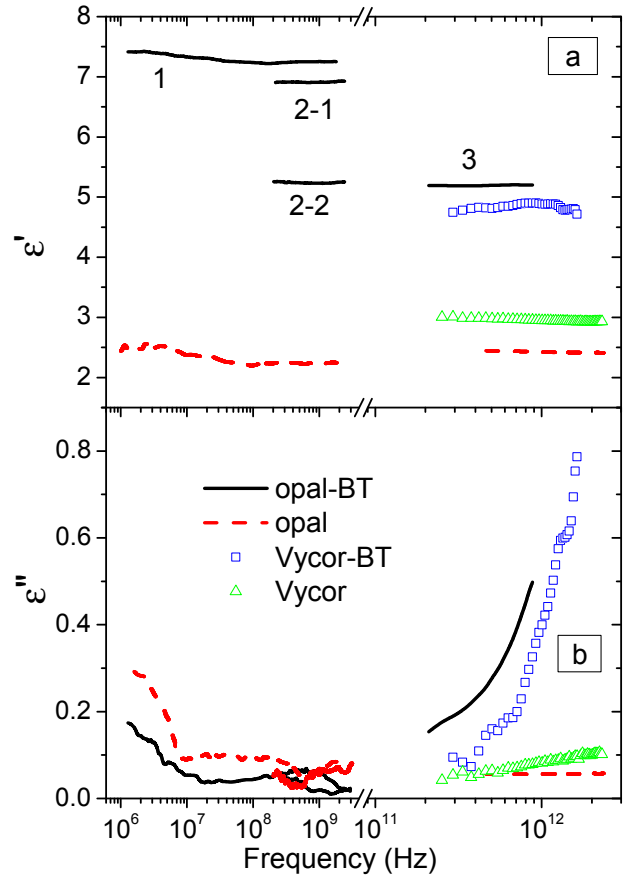


Figure 6. Room temperature broad-band dielectric spectra of Vycor-BT and opal-BT composites compared to those of both empty matrices. Curves 1 (10^6 – $1.8 \cdot 10^9$ Hz) are obtained by the coaxial impedance technique, curves 2 ($2 \cdot 10^8$ – $4 \cdot 10^9$ Hz) by the open-end coaxial method and curves 3 ($2 \cdot 10^{11}$ – $2 \cdot 10^{12}$ Hz) by time-domain THz spectroscopy. The two permittivity values measured by the open-end coaxial method are obtained from opposite sides of the opal-BT sample.

into the sample plate. Therefore the resulting permittivity was somewhat higher for the higher BT-concentration sample side attached to the coaxial line (denoted by 2-1 in Fig. 6) than for the lower BT-concentration side (2-2 in Fig. 6). For the coaxial impedance technique, the E -field is perpendicular to the sample surface so that some average BT concentration across the whole sample thickness is detected. Similar effect of averaging over the BT concentration, but with the E -field in plane, is operative in case of the THz transmission, where also whole sample thickness plays a role. The MW losses of all samples are close to the limit of measurability and their weak increase at lower frequencies could be due to residual water content in the pores.

Taking all this into account, a good agreement concerning the permittivity values is attained, including the low-frequency values from our IR reflectivity fits in Figs. 4 and 5. No appreciable permittivity dispersion is observed below THz frequencies, with permittivity values of 5–10 compared to 2.5–3 of the empty glass ma-

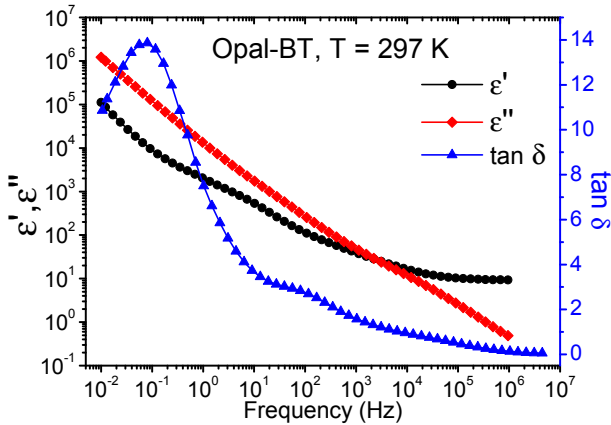


Figure 7. Low frequency dielectric data of the opal-BT sample at room temperature

trices. This picture is consistent with the very low MW losses. On the other hand, in the THz range a steep increase in losses with increasing frequency is seen, obviously due to a ferroelectric soft mode wing, whose characteristic frequency (loss maximum) is near 90–100 cm^{-1} (~ 3 THz) in all our spectra in Fig. 4.

To complement our dielectric spectroscopy data on opal-BT sample, we performed also standard low-frequency capacitance measurements with sputtered Au electrodes. The results at room temperature are present-

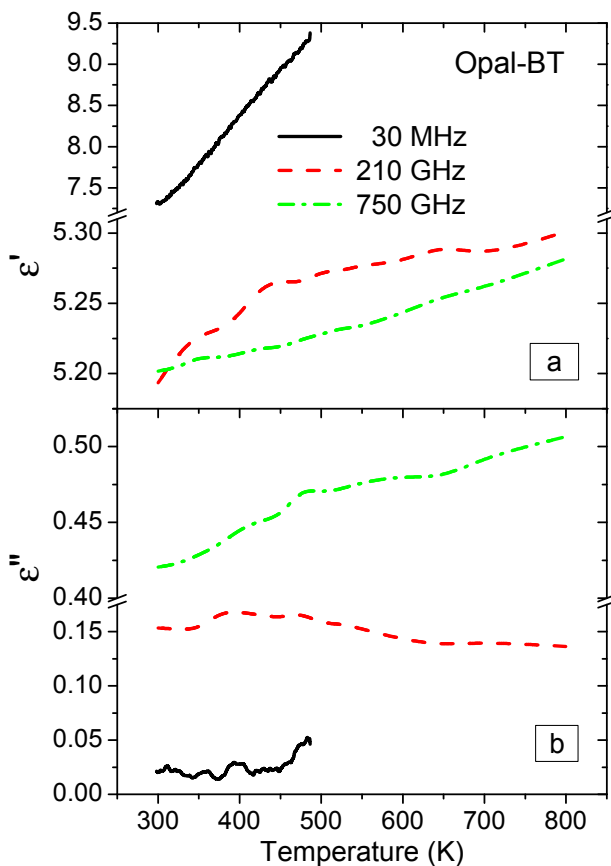


Figure 8. Temperature dependence of the THz and MW data of the opal-BT sample at three characteristic frequencies. No evidence of the ferroelectric transition can be seen.

ed in Fig. 7. It is seen that below ~ 1 kHz a strong dielectric dispersion sets in, which yields a very high maximum in $\tan\delta$ near 0.1 Hz. This dispersion (similar to that observed in other similar nanocomposites [14,15,24]) is dependent on the sample history and is obviously due to some Maxwell-Wagner-type mechanism (sample-electrode and BT particle silica interphases), which is beyond the scope of our discussion in this paper.

In Fig. 8 we present our results of temperature dependences, performed using the coaxial impedance technique in the 300–480 K range and THz technique in the 300–800 K range. The dependences for three characteristic frequencies are plotted, showing only slight monotonous dependences without any ferroelectric transition anomaly. Also differential scanning calorimetry did not reveal any phase transition anomaly from 300 to 500 K. We have performed also the temperature dependences of capacitance measurements, which are more accurate and sensitive on losses than the MW techniques. The results, presented on cooling from 680 K in Fig. 9 for 100 kHz (without appreciable dispersion from 1 kHz to 1 MHz), are in good agreement with the higher-frequency data, showing however a very small and broad permittivity maximum near 400 K, which could indicate a smeared ferroelectric transition. The increase in permittivity as well as in losses at temperatures above ~ 550 K is a usual effect connected with an increasing (nano-inhomogeneous) conductivity in the sample and will not be further considered.

To check if BT in our samples really undergoes a ferroelectric phase transition (as slightly indicated from the permittivity data in Fig. 9), we performed Raman scattering measurements of our samples. Room temperature spectra are shown in Fig. 10 (empty glass matrices give only weak Raman response and are not shown). Whereas the Vycor-BT sample shows only broad features, which obviously characterize the amorphous phase consistent with the IR reflectivity and XRD, and the opal-BT-poor sample side is dominated by some lu-

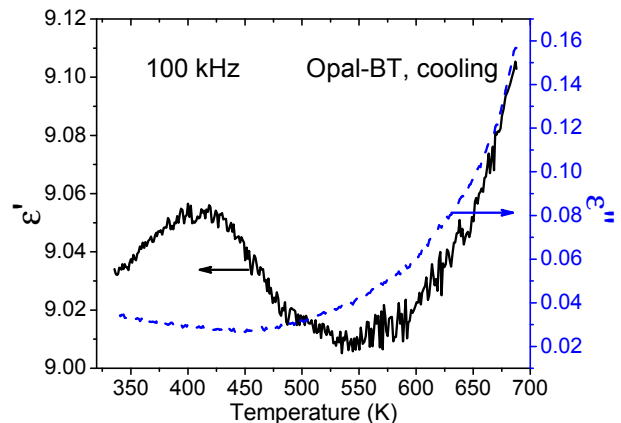


Figure 9. Temperature dependence of the complex dielectric permittivity of the opal-BT sample at 100 kHz, obtained on cooling

minescence features (not shown), the opal-BT-rich side shows features of BT spectra in the ferroelectric phase, characterized by small sharp peaks at 182 and 305 cm^{-1} , clearly assigned to IR active TO_2 and silent TO_3 mode, respectively [25,26].

For the opal-BT sample, we investigated the changes of the Raman spectra on heating in order to see whether these sharp features vanish at higher temperatures, as expected at the ferroelectric transition to a paraelectric phase (the broad TO_1 and TO_4 peaks near 270 and 520 cm^{-1} persist above $T_c \approx 400$ K even in BT single crystals [25]). The temperature dependence was measured up to ~ 520 K, with the sample in a variable-temperature Linkam cell and the spectrometer fitted with a grating Rayleigh filter to include the low-frequency part down to ~ 15 cm^{-1} . The results are shown in Fig. 11. It appeared that two sharp features were faintly discernible even at the highest temperatures. Hence, careful analysis of the measured spectra was performed to account quantitatively for their temperature dependence. To this end, the spectra were corrected for the temperature factor, normalized by total integrated area, and fitted by a sum of independent harmonic oscillators, complemented with a coupled oscillator pair for the two strongest asymmetric A_1 peaks (TO_1 and TO_4) at ~ 270 and ~ 520 cm^{-1} [25]. An example of the fit is shown for the 300 K spectrum in the bottom part of Fig. 11, where the individual component peaks are superimposed on a constant background. The two sharp TO_2 and TO_3 peaks are very clearly seen. Their contributions to the spectra at different temperatures are best visualized in Fig. 12 where the plots of “residuals” show the experimental data after subtraction of all other fit components. As shown in Fig. 13, their total Raman strength (integrated peak area) decreases monotonously with temperature; only at the highest temperature the amplitudes (in particular that of TO_1) start to merge into the noise level. These results indicate that the ferroelectric phase in the crystalline BT in our opal-BT sample does not fully vanish up to $T \sim 520$ K so that the phase transition takes place in a rather diffuse form and with some thermal hysteresis, as evidenced by slightly different strengths of the TO_2 and TO_3 modes on cooling (not shown).

Let us now discuss the Vycor-BT sample with amorphous BT. The amorphous phase is confirmed not only by XRD (Fig. 2), but also by IR reflectivity and Raman spectra, which do not show the sharp TO_2 mode near 180 cm^{-1} (see Figs. 3, 4, 10), unlike the BT-rich side of the opal-BT sample. On the other hand, the other broader spectral features are still present in both IR and Raman spectra. The assignment of these features is as follows (see e.g. [18–20,25,27], see also our model spectra and BT nanoceramic spectra in Fig. 5): The low-frequency maximum near 100 cm^{-1} corresponds to the stiffened ferroelectric soft mode

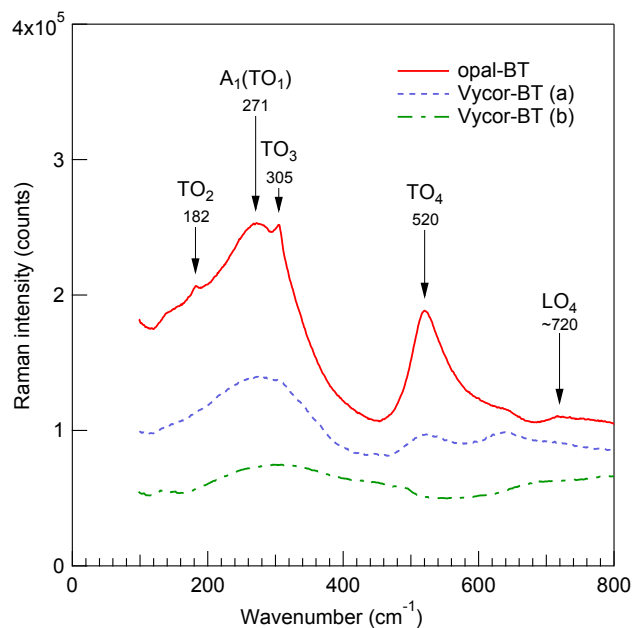


Figure 10. Room temperature Raman spectra from the Vycor-BT sample (two different spots (a) and (b) are chosen) and opal-BT sample from the BT-rich side

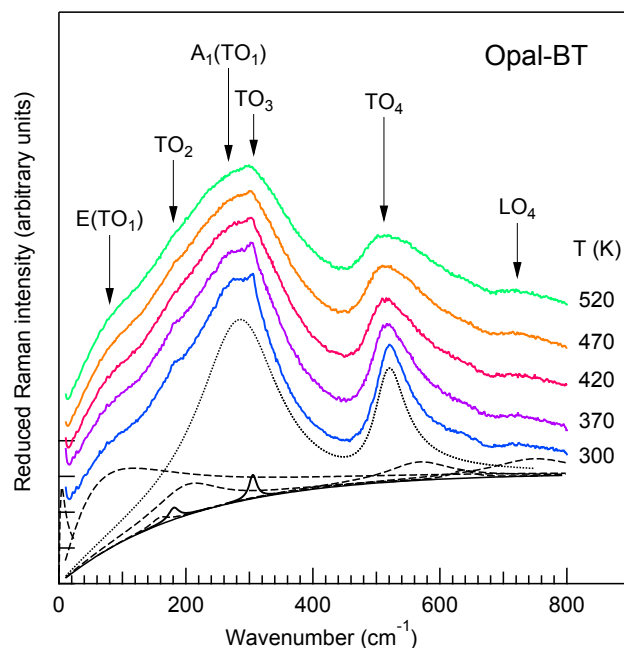


Figure 11. Temperature dependence of the Raman spectra (reduced by the thermal factor and normalized by total area) of the opal-BT sample from the BT-rich side.

Decomposition into individual contributions superimposed on a (reduced) constant background is shown for the spectrum taken at 300 K. Dashed lines represent single oscillator contributions, dotted line is the coupled oscillator pair (TO_1 , TO_4), whereas small sharp peaks at ~ 180 and 302 cm^{-1} corresponding respectively to TO_2 and TO_3 are emphasized by solid lines.

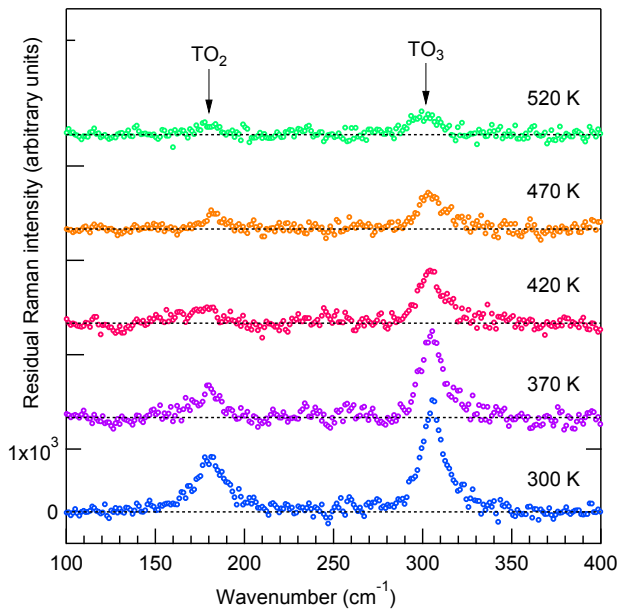


Figure 12. Visualization of the contribution of TO_2 and TO_3 peaks after subtraction of all other components of the fit from the experimental data of Fig. 11

($E(TO_1)$), whose eigenvector consists essentially of Ti vibrations against the O-octahedra perpendicularly to P_s or local octahedra dipole moment in the case of no long-range ferroelectric order. The next broad feature 270–300 cm^{-1} corresponds to the A_1 component of the same vibration (so-called Slater mode) but along P_s or local dipole moment in the TiO_6 octahedra. The last broad feature at 500–600 cm^{-1} corresponds to oxygen octahedra stretching (so called Axe mode [27]). All these modes belong in fact to internal $Ti-O_6$ octahedra vibrations. Their presence even in the amorphous BT shows that the TiO_6 octahedra exists even in the amorphous phase and the huge $E-A_1$ splitting of the TO_1 mode shows that the octahedra are ferroelectric-like distorted even in the amorphous phase, i. e. the Ti ions are off-centered. Absence of the sharp TO_2 mode, which represents the vibrations of Ba ions against the

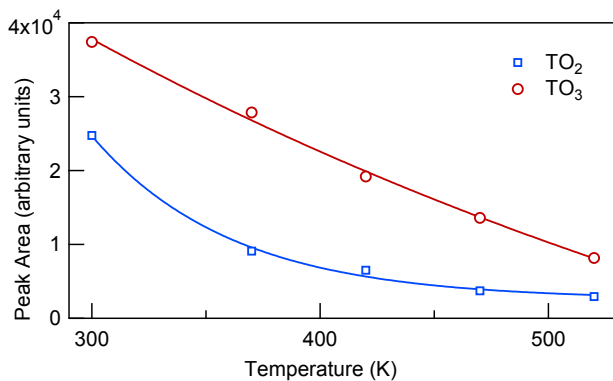


Figure 13. Temperature dependence of the total Raman strength (peak area) of the TO_2 and TO_3 modes in the opal-BT Raman spectra. The solid curves are guides to the eye

TiO_6 octahedra (so called Last mode), clearly indicates absence of the long-range order as expected for the amorphous phase.

The presence of the TO_2 mode in the IR and Raman spectra of our opal-BT sample from the BT-rich side (Figs. 3, 4 and 10) is characteristic for the crystalline BT phase, as also seen in XRD (Fig. 2). But its absence from the BT-poor side of our sample indicates a strong gradient of the crystalline BT concentration from the surface inside the sample. This might be caused by the complicated topology and shape of the opal pores with possible narrow bottlenecks for penetrating the BT sol. From the absence of crystalline BT in the Vycor-BT sample it follows that the formation of crystalline BT is possible only in broader pore channels of diameter larger than ~ 6 nm. Concerning the amorphous BT phase, our spectra indicate also some depth concentration gradient (see the small difference of the permittivity evaluated from the low-frequency end of IR reflectivity ($\epsilon \approx 6$) and THz transmission ($\epsilon \approx 5$) in Figs. 4 and 6), but certainly smaller than in the case of crystalline BT. More quantitative conclusions on the BT concentration gradient is hard to give from our data, neither on ratio of the crystalline nor amorphous part of BT.

Let us now discuss the absence (or its very small magnitude in Fig. 9) of dielectric anomaly near the ferroelectric transition, whose existence was revealed from the Raman spectra. Similar features have been recently observed in a PVDF-BT nanocomposite with BT powder particles of ~ 7 nm embedded into a PVDF polymer matrix [24]. The reason for this absence, even if the particles undergo a ferroelectric transition, is stiffening of the effective soft mode and blocking of its softening on approaching the ferroelectric transition because of the ac depolarizing electric field acting on particle boundaries [28]. Only in macroscopically percolated clusters of the ferroelectric particles in the direction of the ac field, depolarizing field is zero and such part of the composite could show the mode softening like the bulk ferroelectric sample. The absence of such features in our THz spectra shows that there are no such clusters in our composite. It means that BT forms only isolated nanoparticles in the pores of our opal sample without any interconnected percolation, which could be expected in view of the narrow bottlenecks in the opal pores.

In addition to application aspects in nanoelectronics, there are two basic purposes of studying the ferroelectric nanocomposites: to discuss the size effect of the ferroelectric phase transition and to reveal confinement effects on the phonons. Our results and their discussion show that, owing to the depolarizing field effects, it is rather difficult to reveal the intrinsic size effect on the ferroelectric transition. Anyway, the size effect may strongly depend on the particle surroundings, as now proved also by first-principles calculations [29]. Con-

cerning the phonon confinement, spectroscopic studies of a similar nanocomposite of porous silica glass and NaNO_2 ferroelectric [15] (pore channels of ~ 7 nm) did not reveal any appreciable phonon confinement except for the polar phonon stiffening due to the depolarizing field. Also in our case it appears that the intrinsic effect is negligible.

V. Conclusions

To study the phonon confinement and ferroelectric size effect, we succeeded to prepare for the first time composites of BT infiltrated into nanoporous Vycor and opal silica matrices. In the former case (pore diameter up to ~ 6 nm) only amorphous BT phase was present, whereas in the latter case (pore diameter up to ~ 50 nm) a combination of amorphous and crystalline ferroelectric phase with a pronounced depth concentration gradient (penetration depth of the order of ~ 0.1 mm) was revealed. A smeared ferroelectric phase transition without any appreciable size effect was revealed for the crystalline phase. Absence of the phonon mode softening shows that no macroscopically percolated BT clusters exist in our sample. The amorphous phase showed clearly ferroelectric-like distorted TiO_6 octahedra, i.e. presence of the off-centered Ti ions.

Acknowledgements: The work was supported by the COST 539 Action, Academy of Sciences of the Czech Rep. (projects AVOZ 10100520, AV0Z40320502, and KAN 301370701) and Austrian FWF (project No. P19284-N20).

References

- H.P. Hood, M.E. Nordberg, Treated borosilicate glass, *U.S. patent* 2.106.744 (1938), Borosilicate glass, *U.S. patent* 2.221.709 (1940), Method of treating borosilicate glasses, *U.S. patent* 2.286.275 (1942).
- U. Even, K. Rademann, J. Jortner, N. Manor, R. Reisfeld, “Electronic energy transfer on fractals”, *Phys. Rev. Lett.*, **52** (1984) 2164–2167.
- W.D. Dozier, J.M. Drake, J. Klafter, “Self-diffusion of a molecule in porous Vycor glass”, *Phys. Rev. Lett.*, **56** (1986) 197–200.
- B. Nettelblad, G.A. Niklasson, “The dielectric dispersion of liquid-filled porous sintered materials”, *J. Phys.: Cond. Matter*, **8** (1996) 2781–2790.
- B. Nettelblad, G.A. Niklasson, “Dielectric relaxation in liquid-impregnated porous solids”, *J. Mater. Sci.*, **32** (1997) 3783–3800.
- A. Gutina, T. Antropova, E. Rysiakiewicz-Pasek, K. Virnik, Yu. Feldman, “Dielectric relaxation in porous glasses”, *Micropor. Mesopor. Mater.*, **58** (2003) 237–254.
- A. Puzenko, N. Kozlovich, A. Gutina, Ty. Feldman, “Determination of pore fractal dimensions and porosity of silica glasses from the dielectric response at percolation”, *Phys. Rev. B*, **60** (1999) 14348–14359.
- W. Schranz, M.R. Puica, J. Koppensteiner, H. Kabelka, A.V. Kityk, “Heterogeneous relaxation dynamics of nano-confined salol probed by DMA”, *Europhys. Lett.*, **79** (2007) 36003-1/6.
- J. Koppensteiner, W. Schranz, M.R. Puica, “Confinement effects on glass forming liquids probed by dynamic mechanical analysis”, *Phys. Rev. B*, **78** (2008) 054203-1/9.
- J. Koppensteiner, W. Schranz, M.A. Carpenter, “Revealing the pure confinement effect in glass-forming liquids by dynamic mechanical analysis”, *Phys. Rev. B*, **81** (2010) 024202-1/8.
- M.I. Samoilovich, A.F. Belyanin, S.M. Kleshcheva, M.Yu. Tsvetkov, “Investigation of opal nanocomposites for photonic applications, in nanostructures and photon crystals”, pp. 195–258 in *Proceedings of 10th Inter. Conf. High Technology in Russian Industry (Plenary reports)*, Moscow, 2004.
- M.I. Samoilovich, S.M. Samoilovich, A.V. Guryanov, M.Yu. Tsvetkov, “Artificial opal structures for 3D-optoelectronics”, *Microelectron. Eng.*, **69** (2003) 237–247.
- K.M. Rabe, C.H. Ahn, J.-M. Triscone (Eds.), *Physics of Ferroelectrics a Modern Perspective*, in *Topics in Applied Physics* 105, Springer, 2007.
- A. Fokin, Yu. Kumzerov, E. Koroleva, A. Naberezhnov, O. Smirnov, M. Tovar, S. Vakhruhev, M. Glazman, “Ferroelectric phase transition in sodium nitrite nanocomposites”, *J. Electroceram.*, **22** (2009) 270–275.
- E.Yu. Koroleva, D. Nuzhnyy, J. Pokorny, S. Kamba, Yu.A. Kumzerov, S.B. Vakhruhev, J. Petzelt, “The negative phonon confinement effect in nanoscopic sodium nitrite”, *Nanotechnol.*, **20** (2009) 395706-1/7.
- T. Ostapchuk, J. Petzelt, J. Hlinka, V. Bovtun, P. Kuzel, I. Ponomareva, S. Lisenkov, L. Bellaiche, A. Tkach, P. Vilarinho, “Broad-band dielectric spectroscopy and ferroelectric soft-mode response in the $\text{Ba}_{0.6}\text{Sr}_{0.4}\text{TiO}_3$ solid solution”, *J. Phys. Condens. Matter*, **21** (2009) 474215/1-9.
- E. Buixaderas, S. Kamba, J. Petzelt, “Lattice dynamics and central-mode phenomena in the dielectric response of ferroelectrics and related materials”, *Ferroelectrics*, **308** (2004) 131–192.
- T. Ostapchuk, J. Petzelt, M. Savinov, V. Buscaglia, L. Mitoseriu, “Grain-size effect in BaTiO_3 ceramics: Study by far infrared spectroscopy”, *Phase Transit.*, **79** (2006) 361–374.
- J.L. Servoin, F. Gervais, A.M. Quittet, Y. Luspain, “Infrared and Raman responses in ferroelectric perovskite crystals: Apparent inconsistencies”, *Phys. Rev. B*, **21** (1980) 2038–2041.
- J.A. Sanjurjo, R.S. Katiyar, S.P.S. Porto, “Temperature dependence of dipolar modes in ferroelectric BaTiO_3 by infrared studies”, *Phys. Rev. B*, **22** (1980) 2396–2403.
- J. Petzelt, “Infrared and THz spectroscopy of nanostructured dielectrics”, *Process. Applic. Ceram.*, **3** (2009) 145–155.

22. T. Ostapchuk, J. Petzelt, M. Savinov, V. Buscaglia, L. Mitoseriu, “Grain-size effect in BaTiO₃ ceramics: Study by far infrared spectroscopy”, *Phase Transit.*, **79** (2006) 361–374.
23. D. Nuzhnyy, J. Petzelt, I. Rychetsky, V. Buscaglia, M.T. Buscaglia, P. Nanni, “THz and IR dielectric response of BaTiO₃ core-shell composites: Evidence for interdiffusion”, *J. Phys. D*, **42** (2009) 155408/1-8.
24. D. Nuzhnyy, J. Petzelt, I. Rychetsky, S. Veljko, J. Kulek, B. Hilczer, “Time-domain terahertz and infrared spectroscopy of BaTiO₃-PVDF nanocomposites”, *Phase Transit.*, **81** (2008) 1049–1057.
25. A. Chaves, R.S. Katiyar, S.P.S. Porto, “Coupled modes of A₁ symmetry in tetragonal BaTiO₃”, *Phys. Rev. B*, **10** (1974) 3522–3533.
26. J.D. Freire, D.S. Katiyar, “Lattice dynamics of crystals with tetragonal BaTiO₃ structure”, *Phys Rev. B*, **37** (1988) 2074–2085.
27. J. Hlinka, J. Petzelt, S. Kamba, D. Noujni, T. Ostapchuk, “Infrared dielectric response of relaxor ferroelectrics”. *Phase Transit.*, **79** (2006) 41–78.
28. J. Petzelt, J. Hlinka, S. Kamba, T. Ostapchuk, D. Noujni, I. Rychetsky, “Effective infrared response of inhomogeneous ferroelectrics”, *Ferroelectrics*, **334** (2006) 199–210.
29. G. Gerra, A. Tagantsev, N. Setter, “Ferroelectricity in asymmetric metal-ferroelectric-metal heterostructures: a combined first-principles-phenomenological approach”, *Phys. Rev. Lett.*, **98** (2007) 207601-1/4.

